Supporting Information

For

Oxalic acid-functionalized covalent organic frameworks for sustainable and effective europium radionuclides separation from active wastewater

List of contents:

Table S1. Kinetic parameters for sorption of $^{152+154}$Eu onto MT-OX-COF.

Table S2. Parameters of the Freundlich, Langmuir, Temkin, and Dubinin–Radushkevich for sorption of $^{152+154}$Eu onto MT-OX-COF.

Table S3. Thermodynamic parameters for sorption of $^{152+154}$Eu onto MT-OX-COF.

Text. Instruments, Sorption investigations, and MT-COF regeneration

Text. Radioactivity determination and real waste preparations

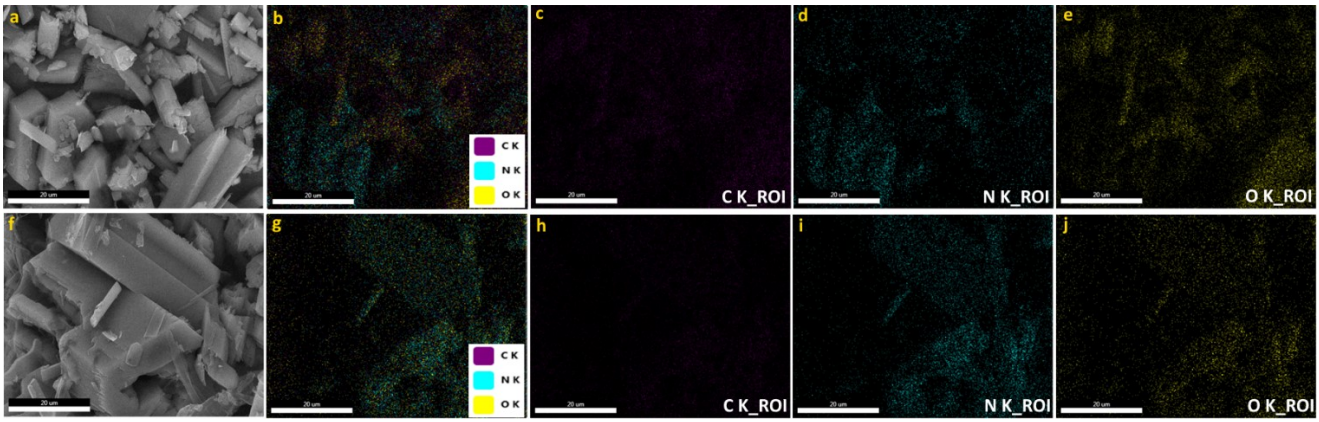

Fig. S1. A single point EDX mapping analysis of: **(a-e)** MT-COF, and **(f-j)** MT-OX-COF.

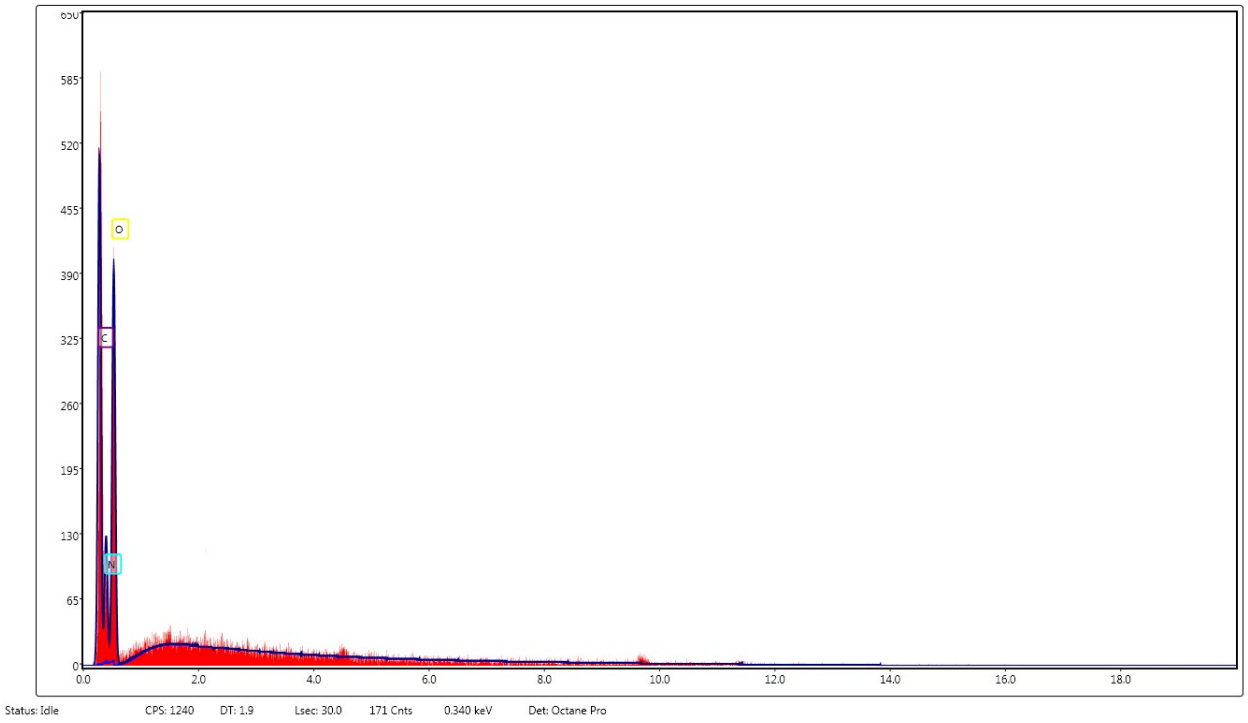

Fig. S2. The energy-dispersive X-ray analysis (EDX) of the MT-COF

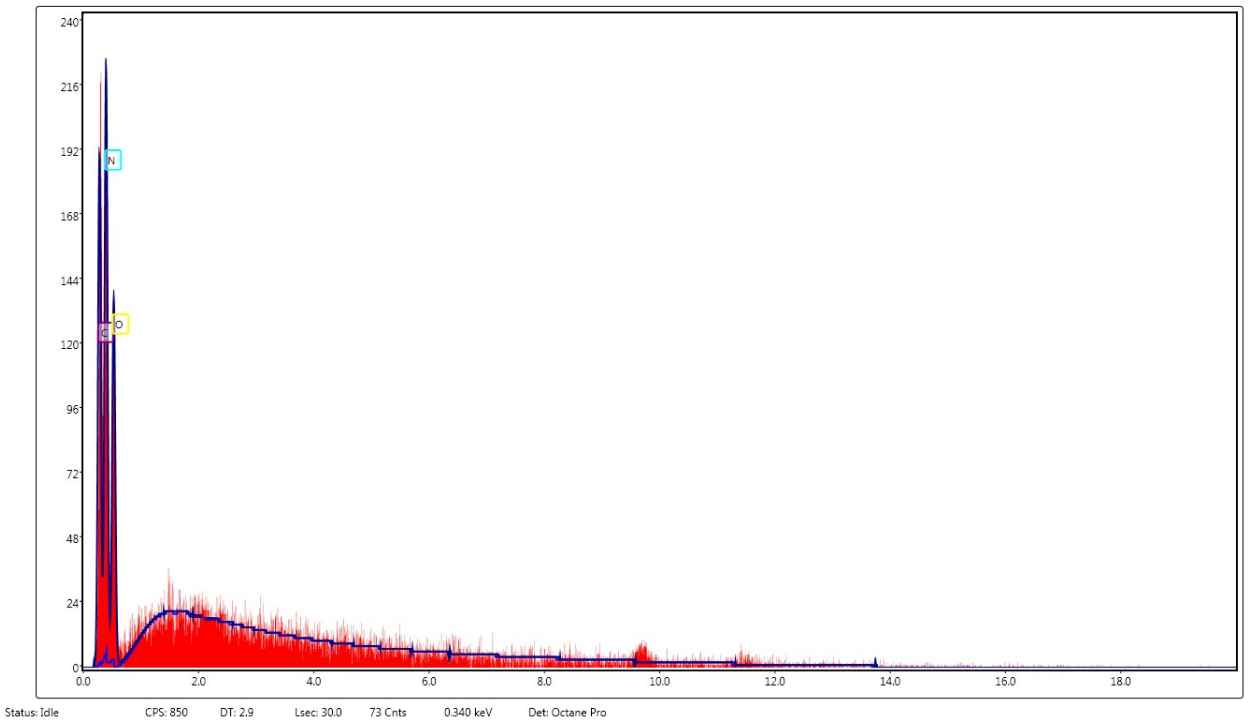

Fig. S3. The energy-dispersive X-ray analysis (EDX) of the MT-OX-COF.

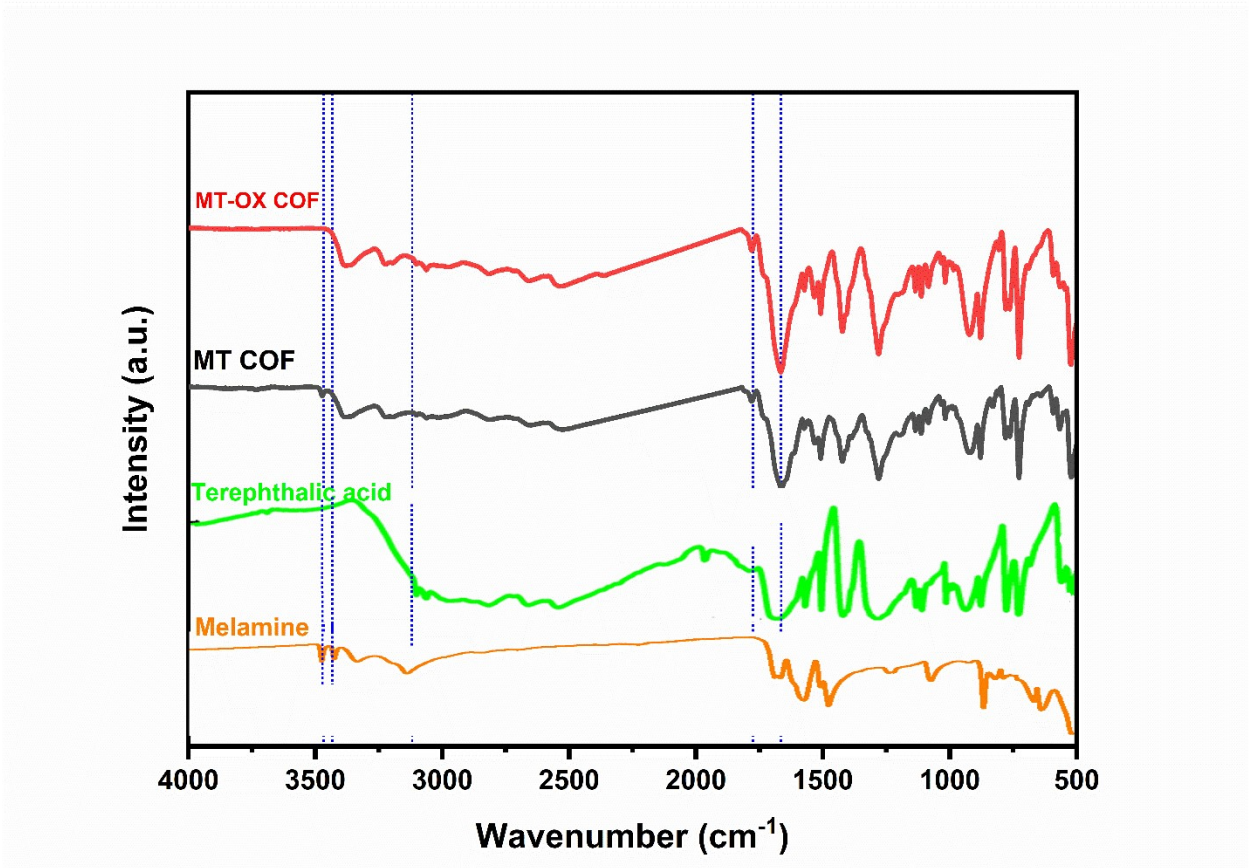

Fig. S4. FT-IR spectra of MT-COF and MT-OX-COF.

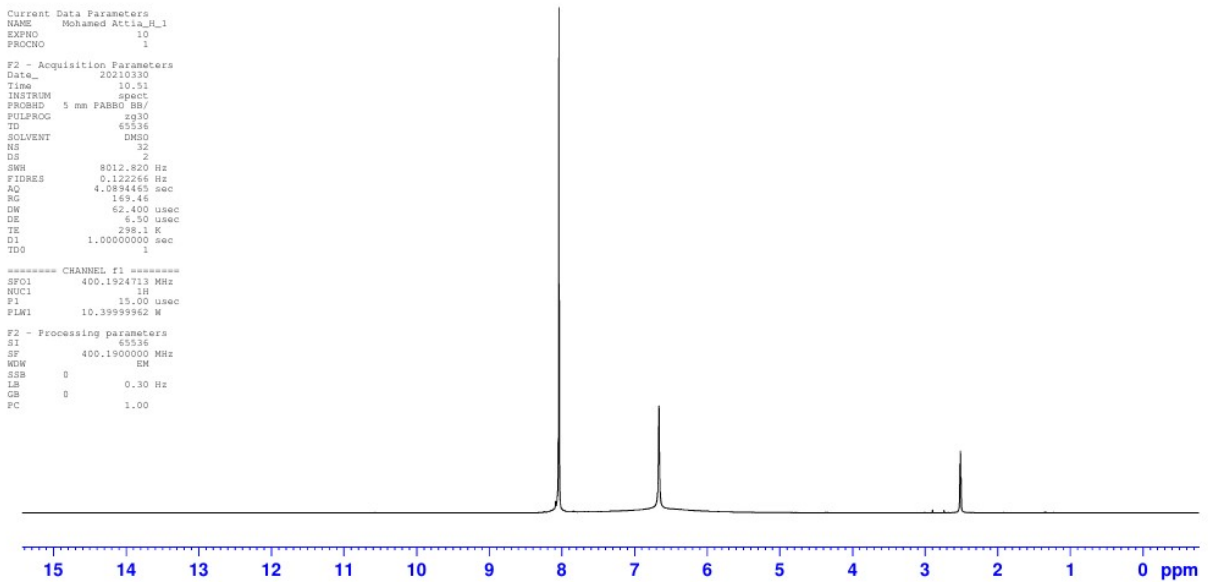

Fig. S5. ^{1}H NMR spectrum of MT-COF.

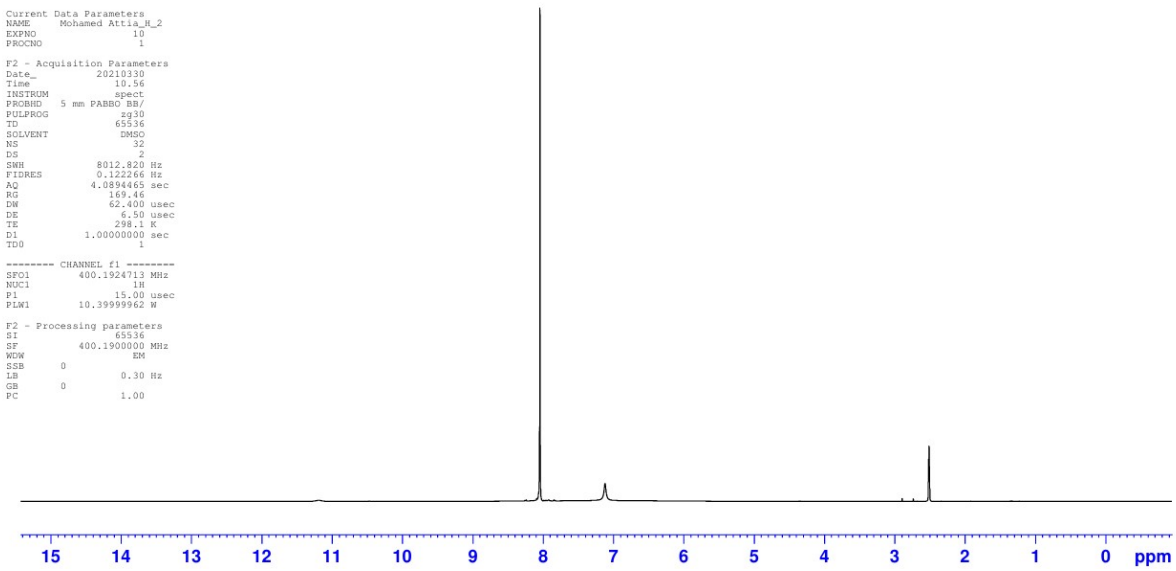

Fig. S6. ^{1}H NMR spectrum of MT-OX-COF.

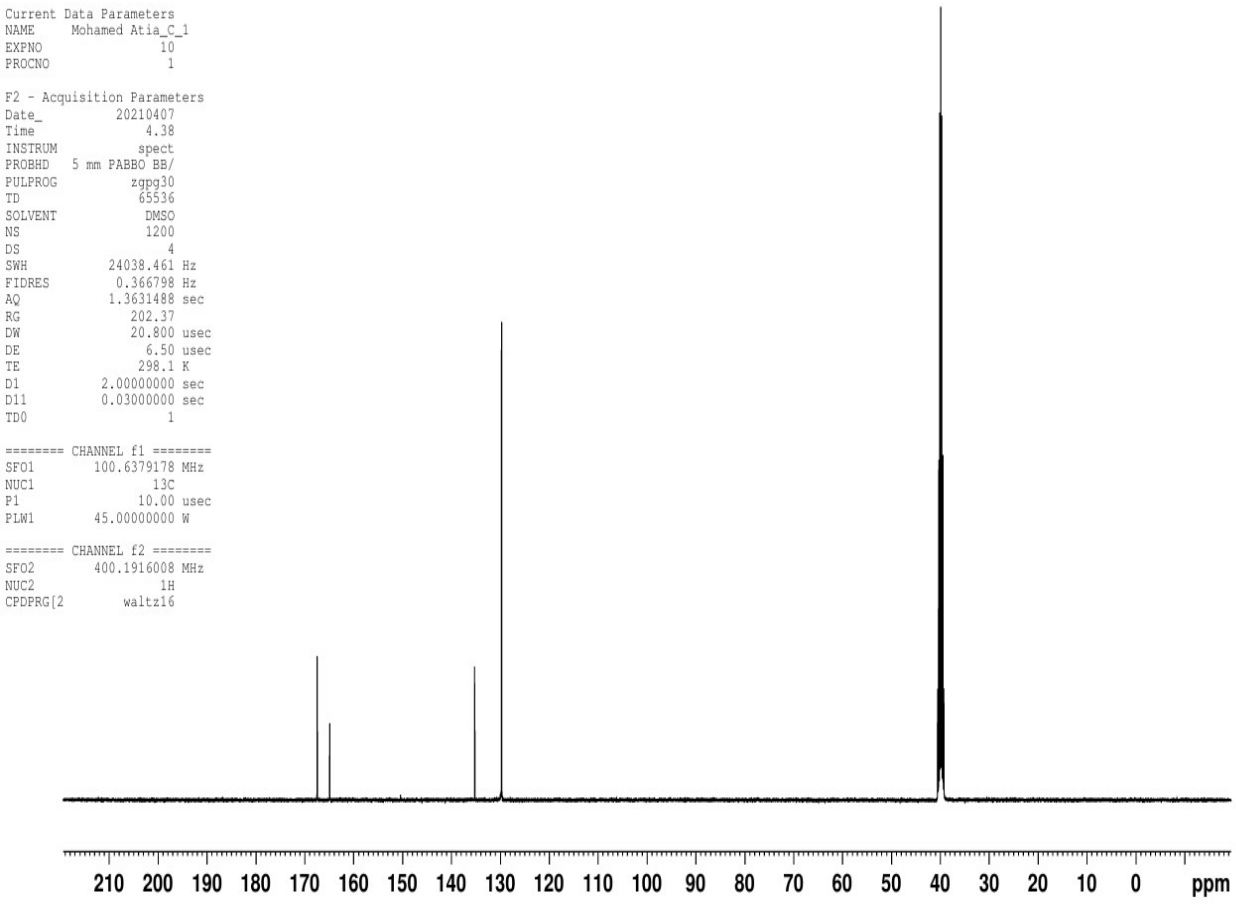

Fig. S7. ^{13}C NMR spectrum of MT-COF.

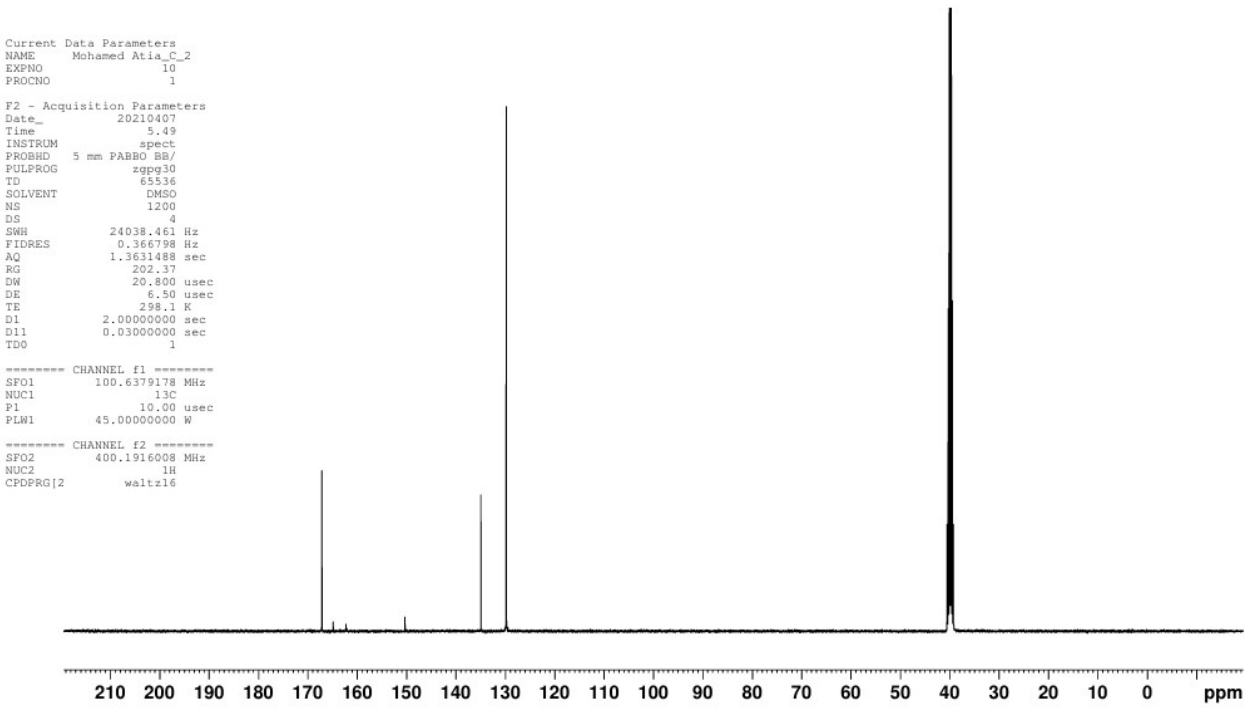

Fig. S8. ^{13}C NMR spectrum of MT-OX-COF.

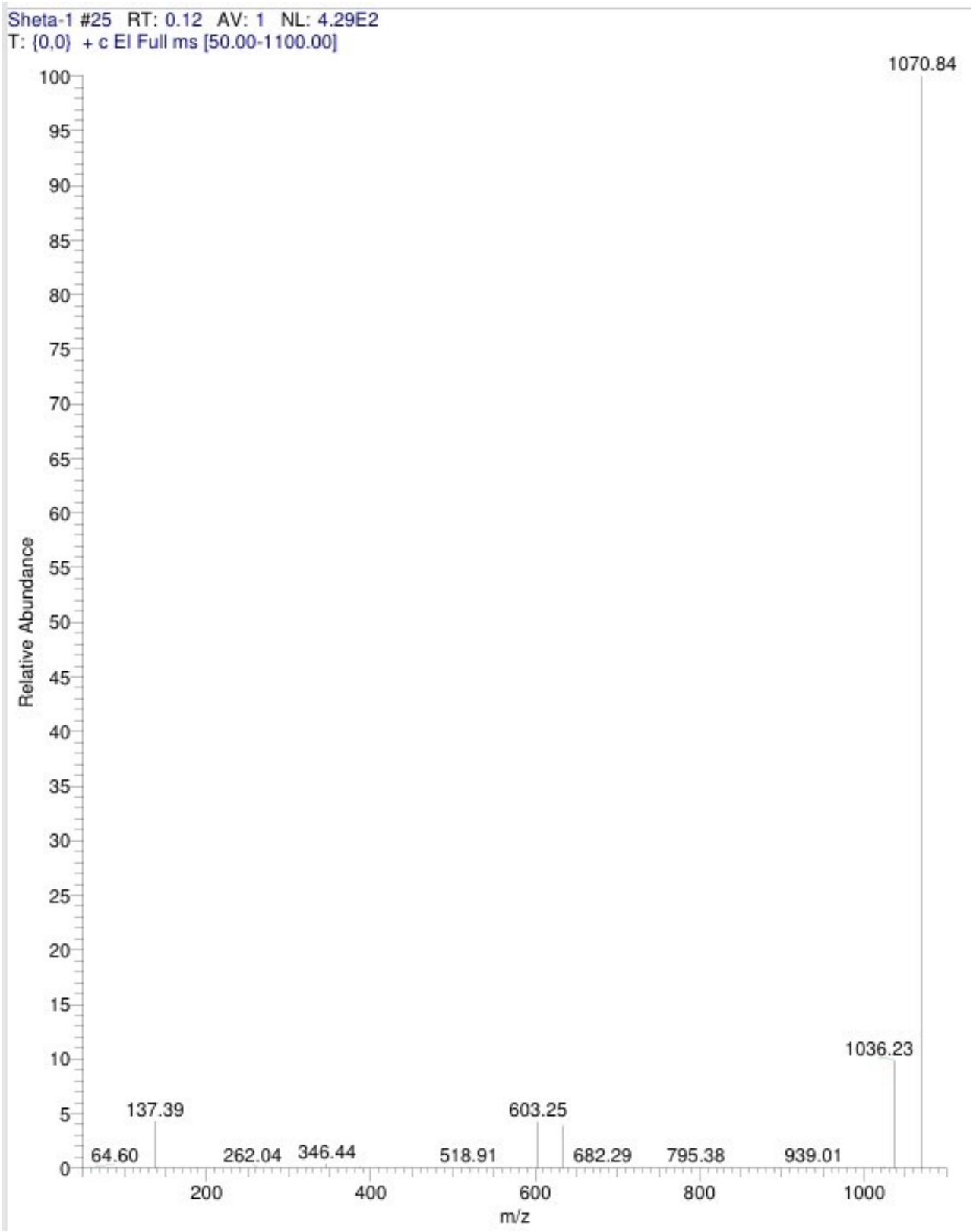

Fig. S9. Mass spectrum of MT-COF.

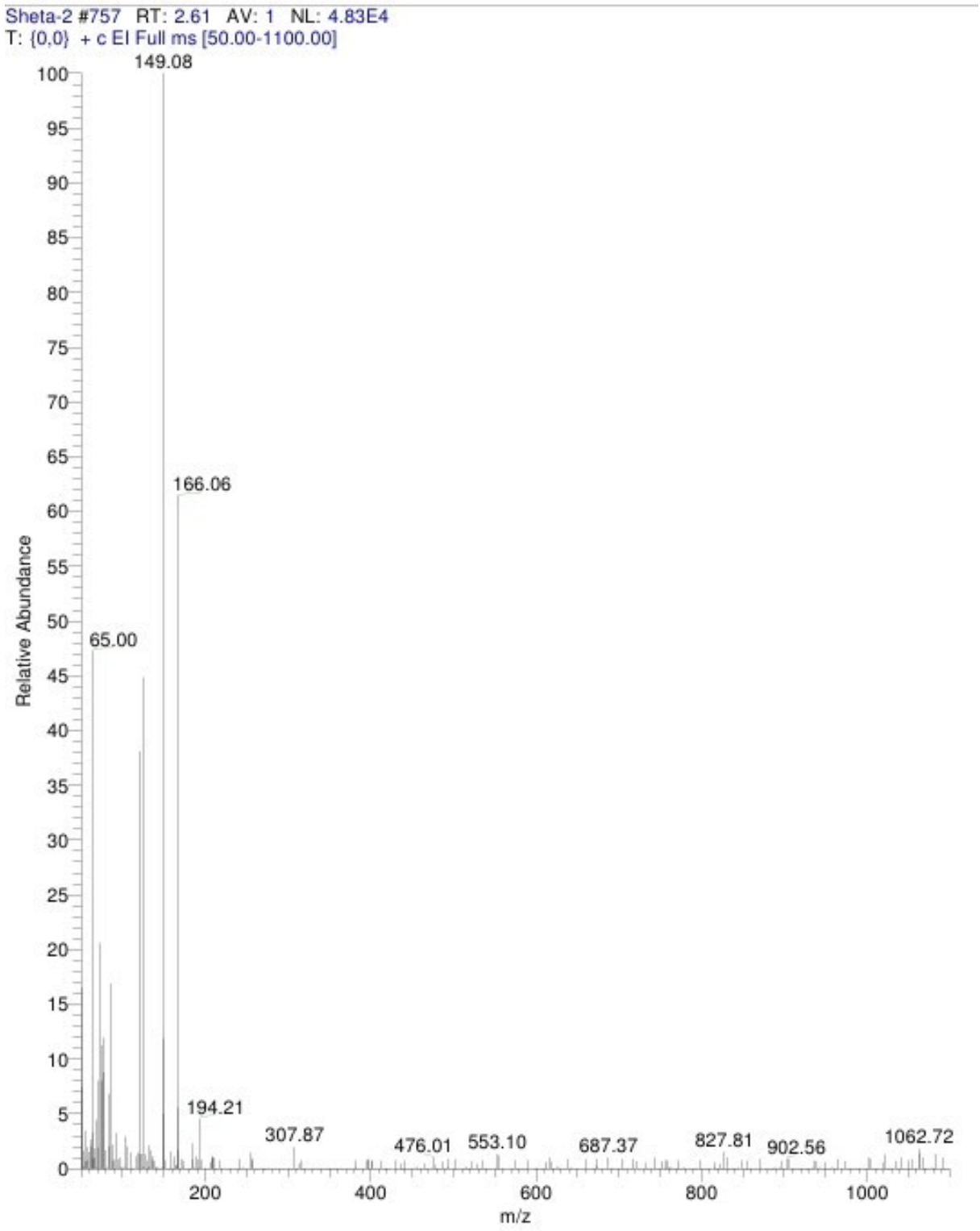

Fig. S10. Mass spectrum of MT-OX-COF.

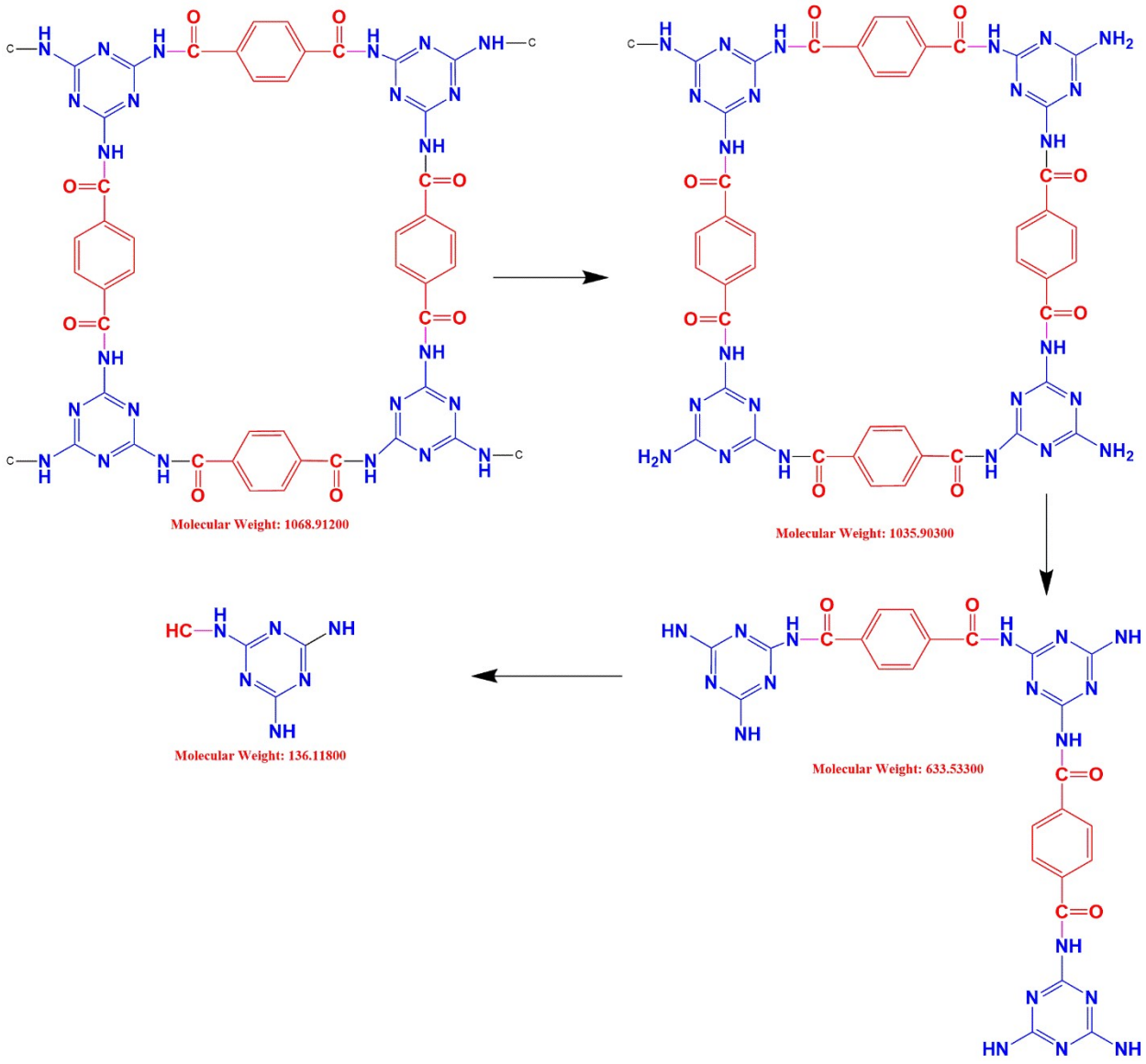

Fig. S11. The proposed mass fragmentation of MT-COF.

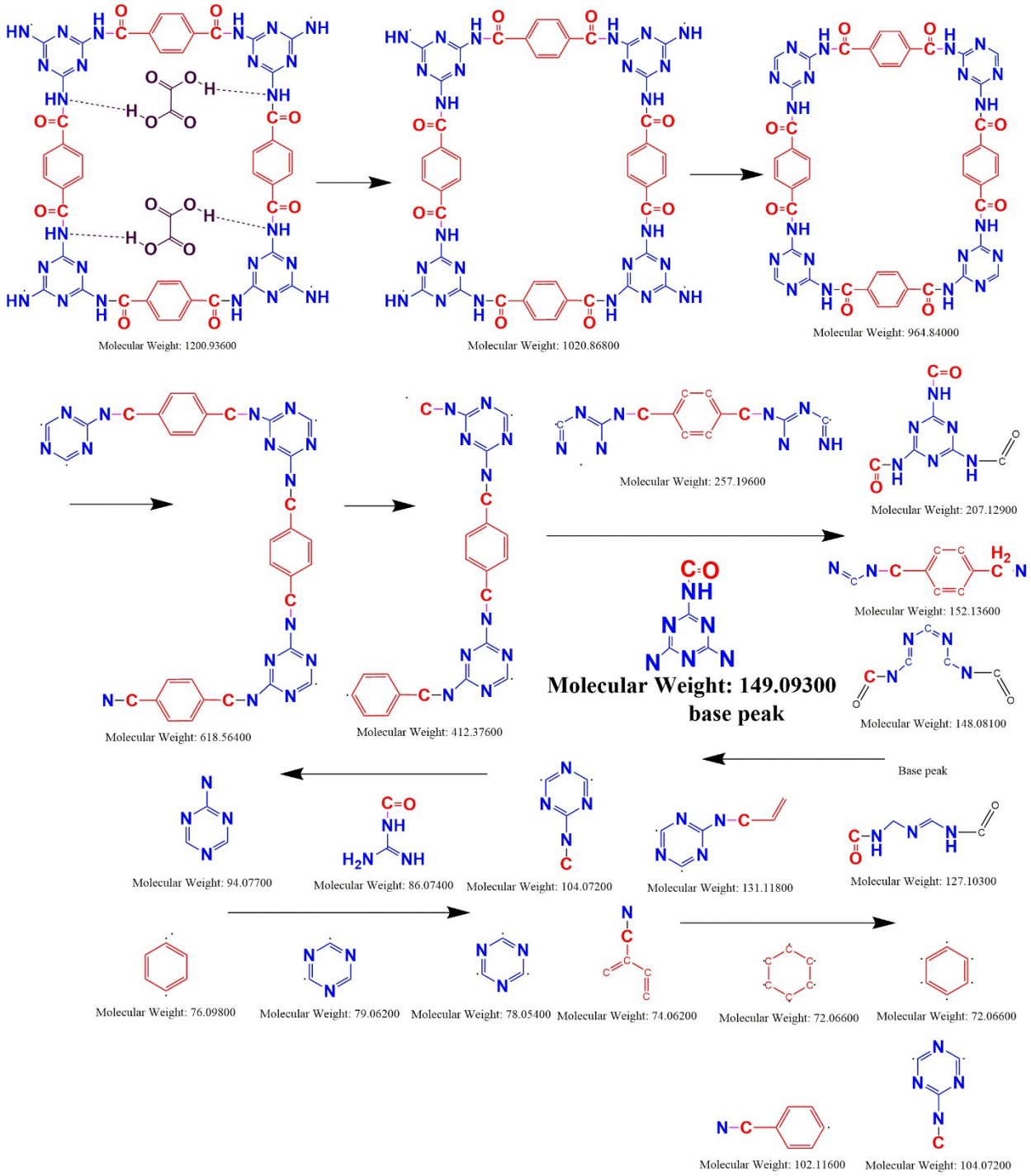

Fig. S12. The proposed mass fragmentation of MT-OX-COF.

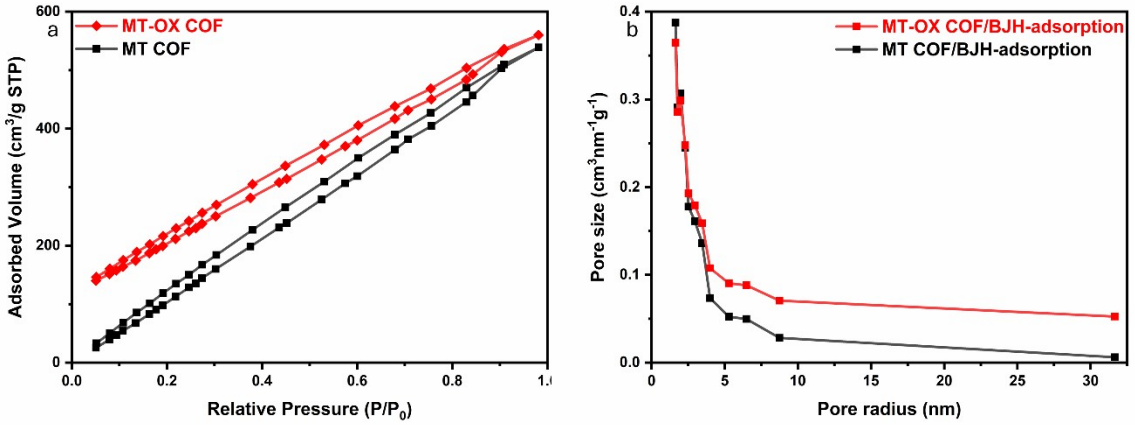

Fig. S13. (a) The N_2 adsorption/desorption isotherms, and **(b)** The changes in pore size distribution to pore radius of MT-COF and MT-OX-COF.

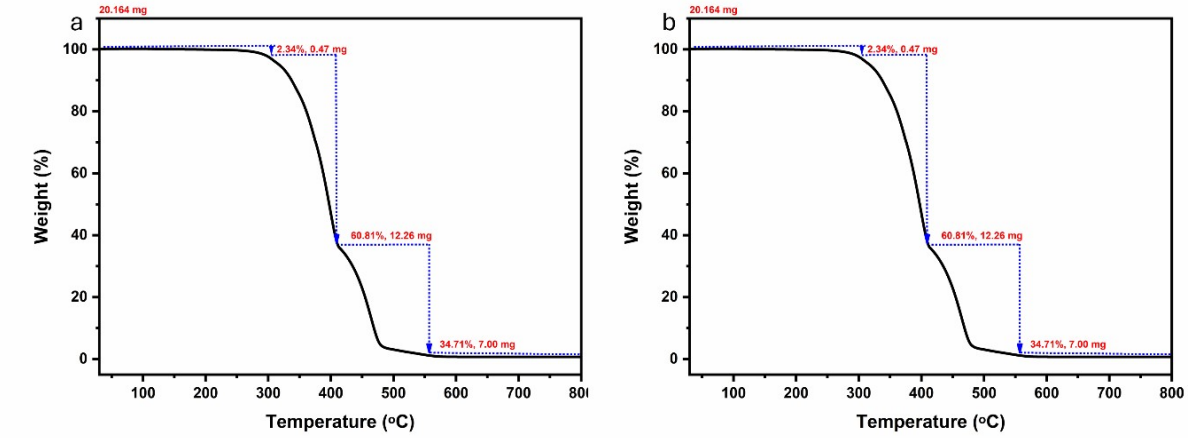

Fig. S14. TGA spectra of: **(a)** MT-COF and **(b)** MT-OX-COF.

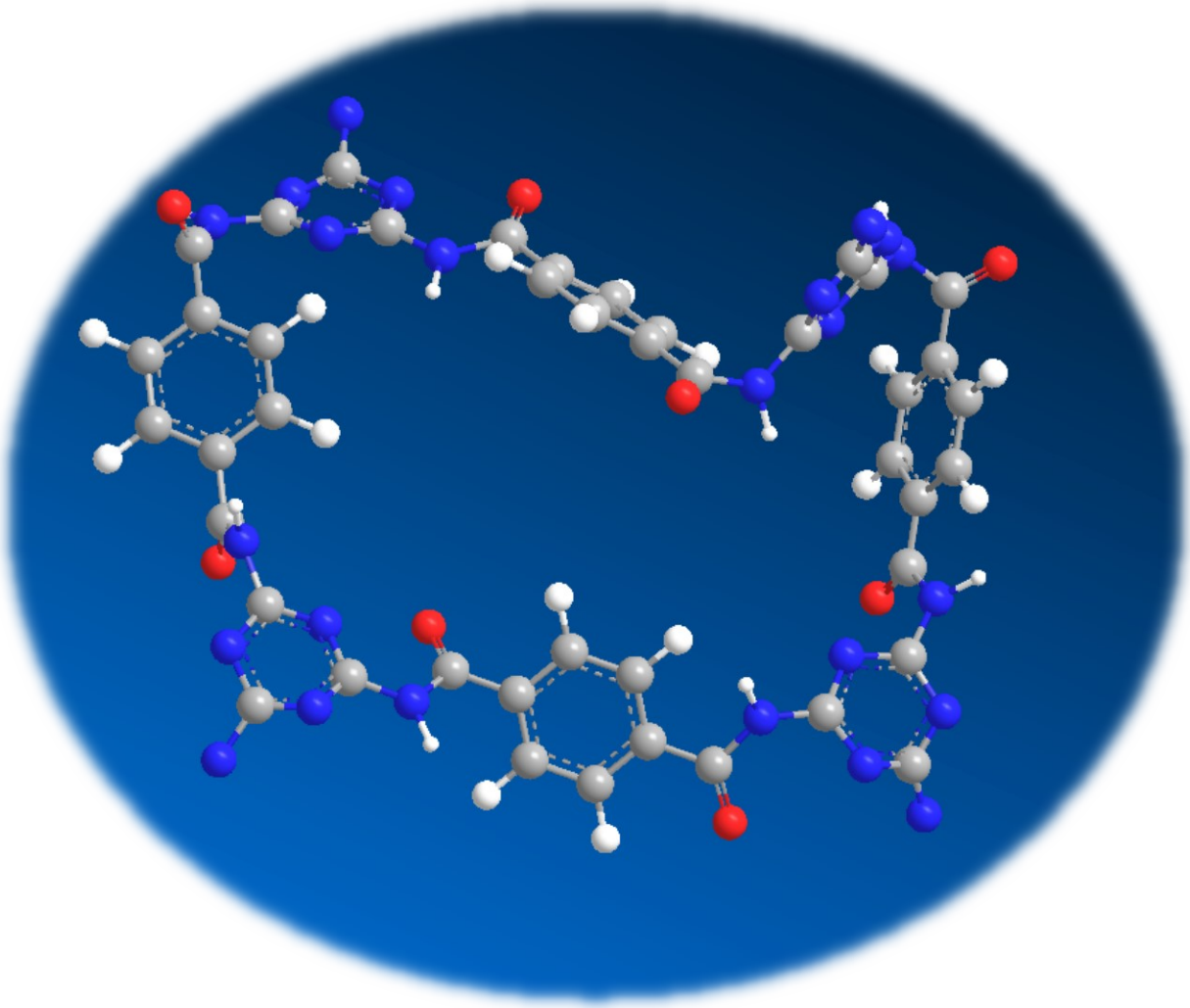

Fig. S15. The 3D Structure of the MT-COF.

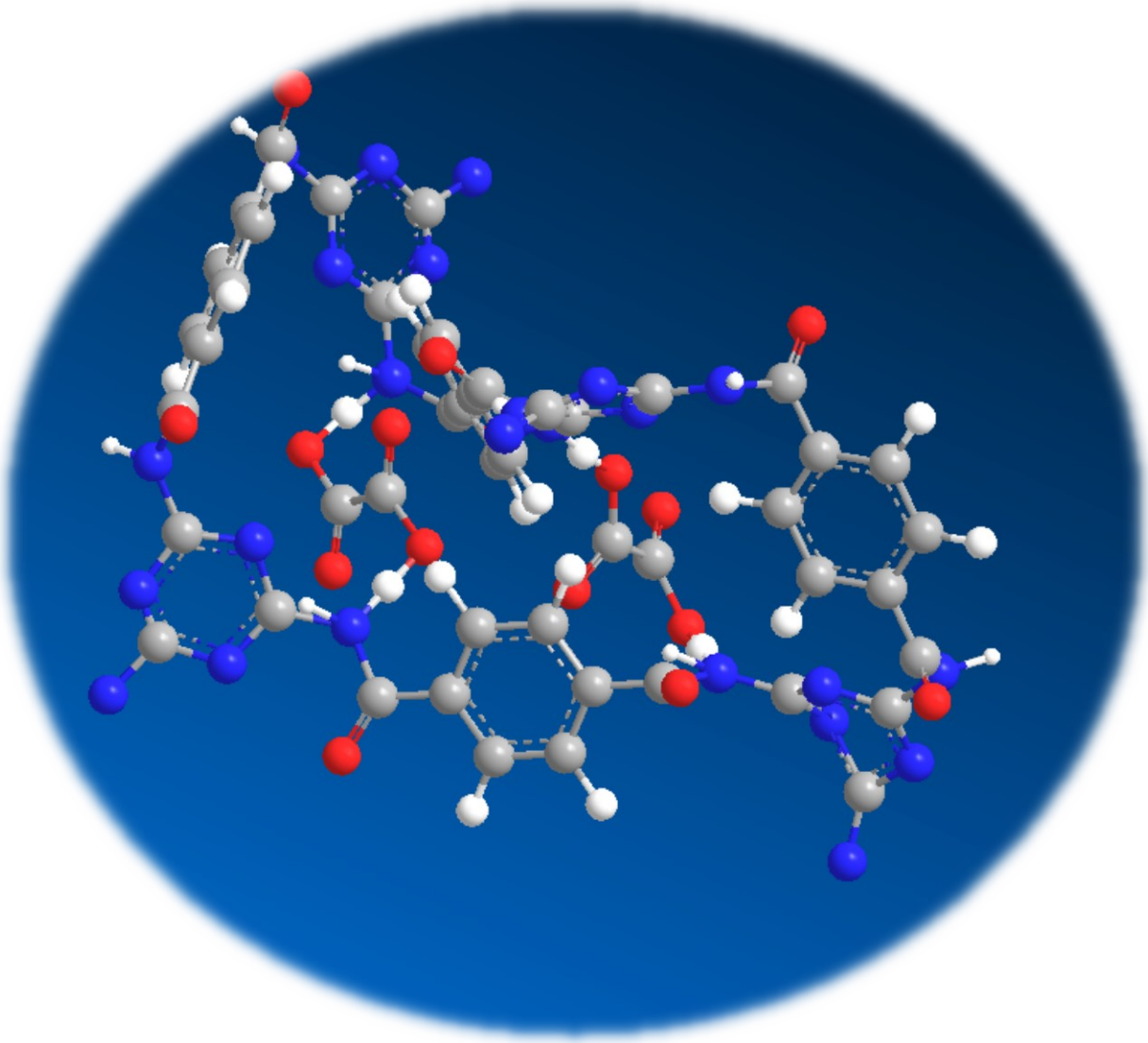

Fig. S16. The 3D Structure of the MT-OX-COF.

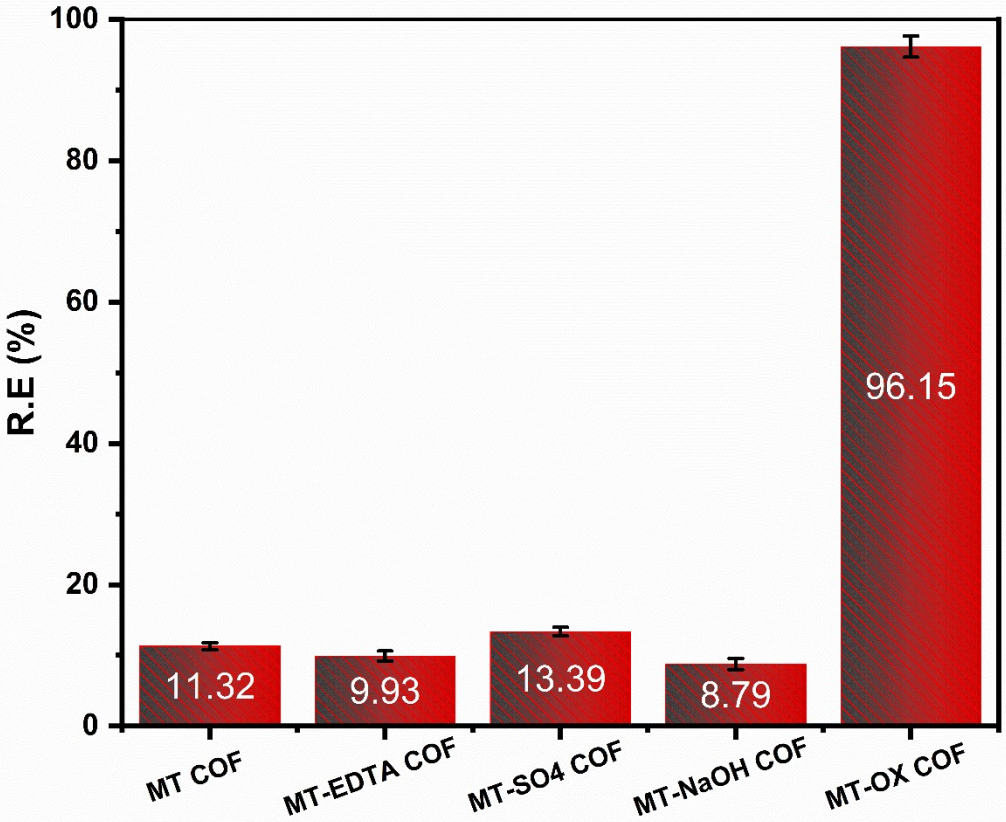

Fig. S17. A comparison between the removal efficiency of MT-COFs.

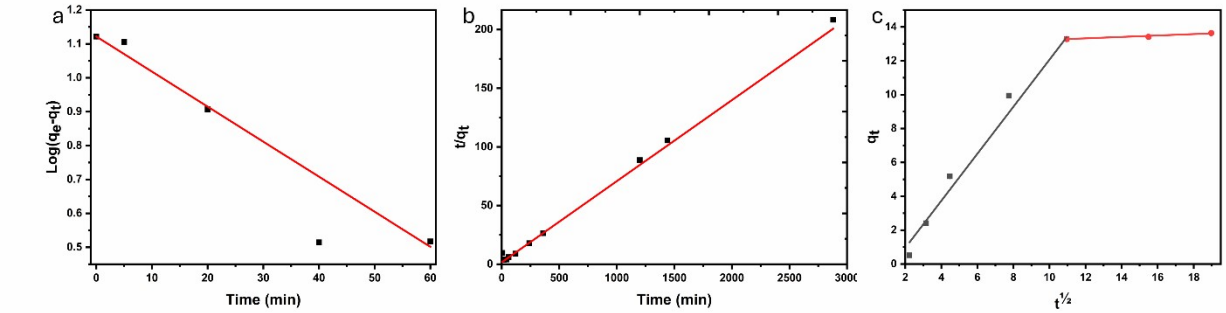

Fig. S18. (a) Pseudo-first-order model, **(b)** Pseudo-second-order model, and **(c)** Intra-particle diffusion plot of $^{152+154}$Eu sorption onto MT-OX-COF.

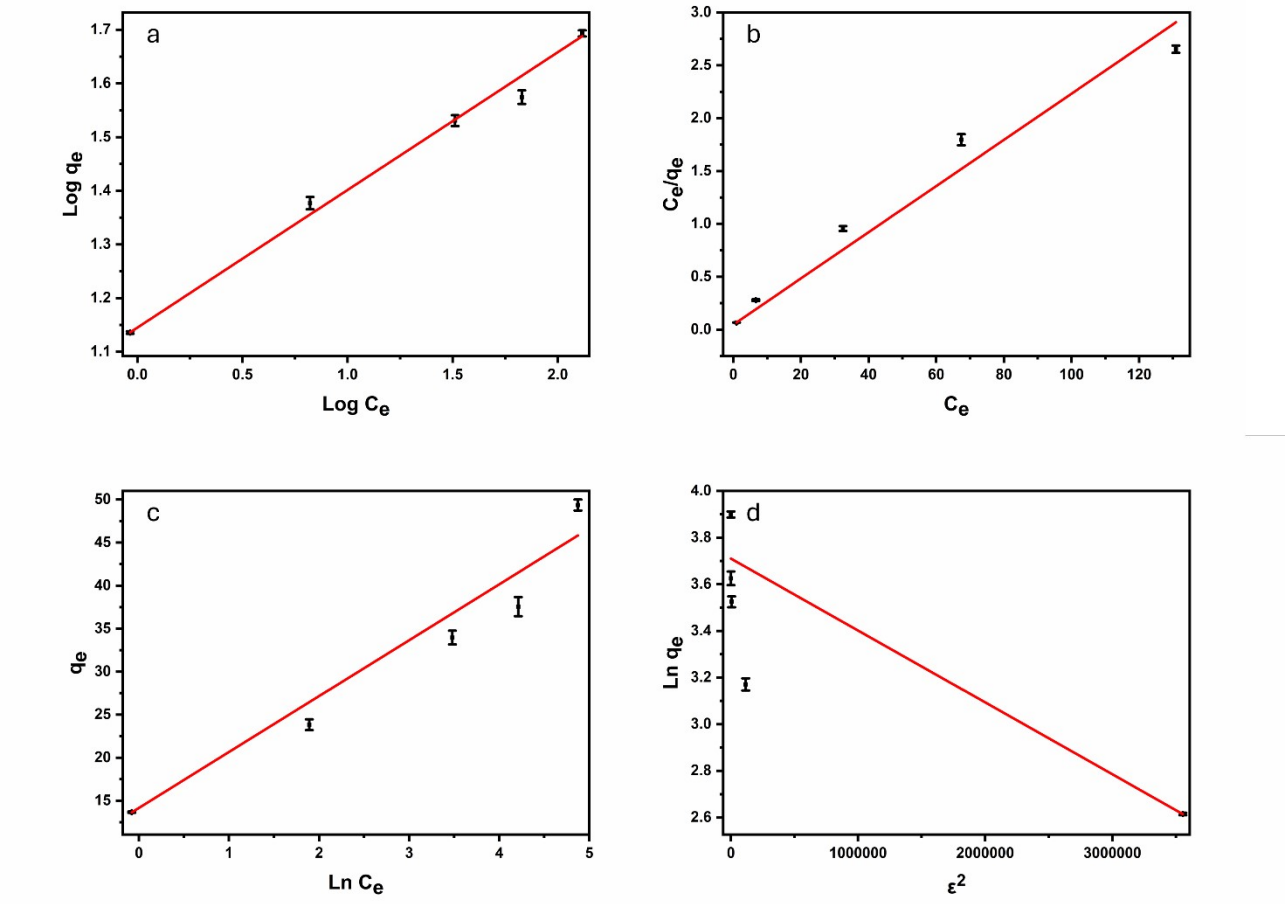

Fig. S19. (a) Freundlich sorption isotherm, **(b)** Langmuir sorption isotherm, **(c)**Temkin sorption isotherm, and **(d)** Dubinin–Radushkevich sorption isotherm at (t_e= 6 h; C_i = (20-200) mg L^{-1}; pH_i = 3.5; V/m= 0.71 L g^{-1}; temp = 25°C) of $^{152+154}$Eu sorption onto MT-OX-COF.

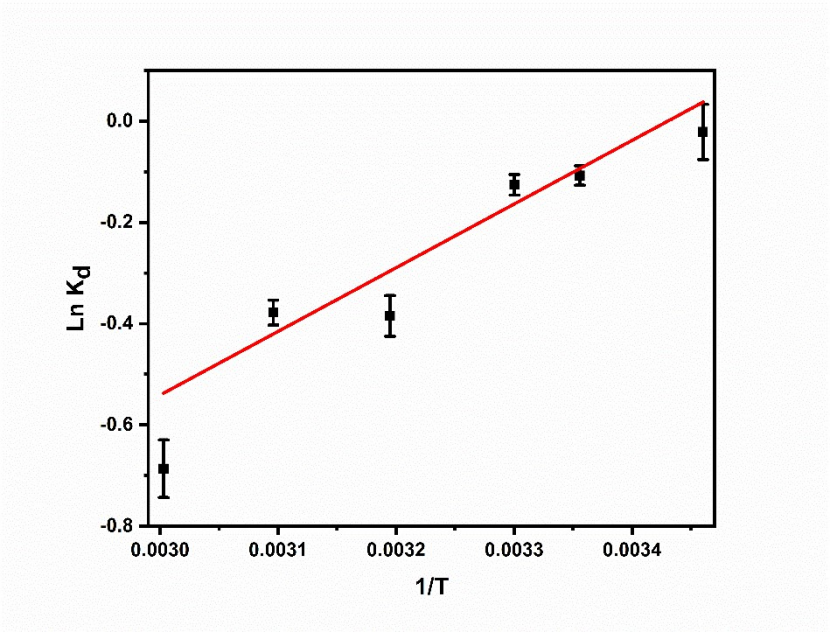

Fig. S20. Thermodynamic study of $^{152+154}$Eu sorption onto MT-OX-COF.

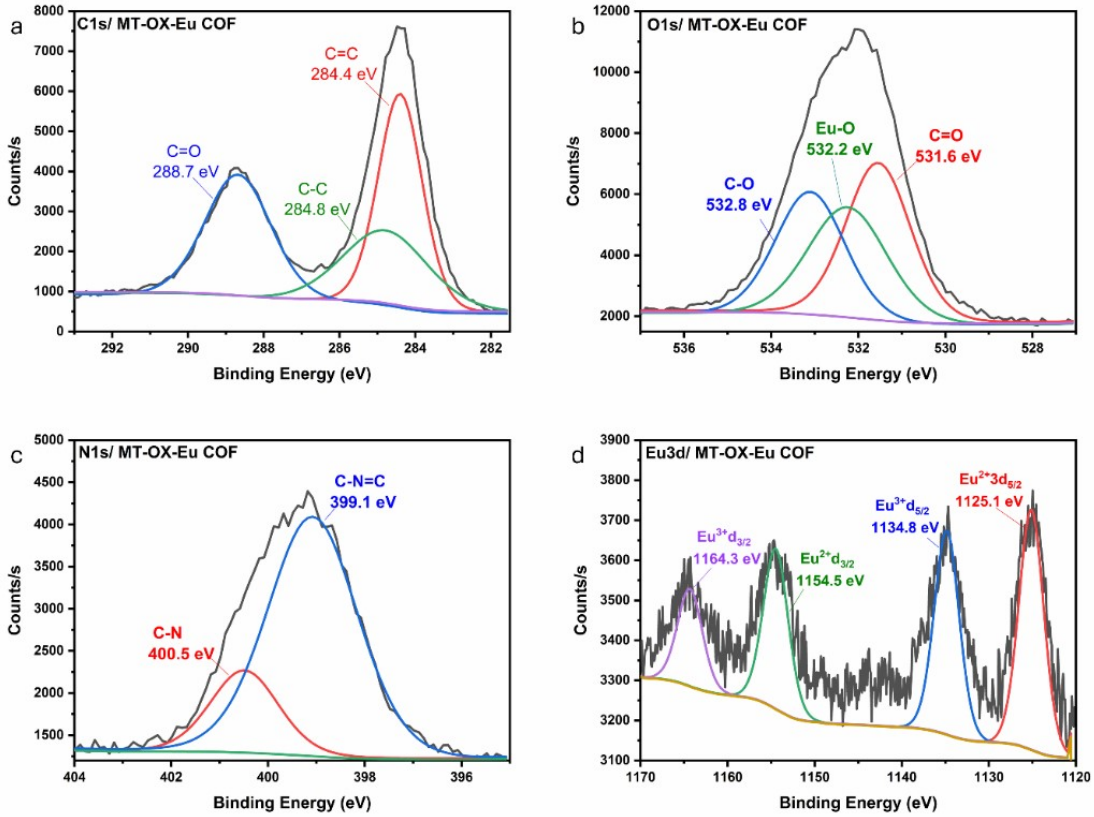

Fig. S21. High-resolution XPS spectra of **(a)** C 1s-MT-OX-COF-Eu, **(b)** O 1s-MT-OX-COF-Eu, **(c)** N1s-MT-OX-COF-Eu, and **(d)** Eu3d-MT-OX-COF-Eu.

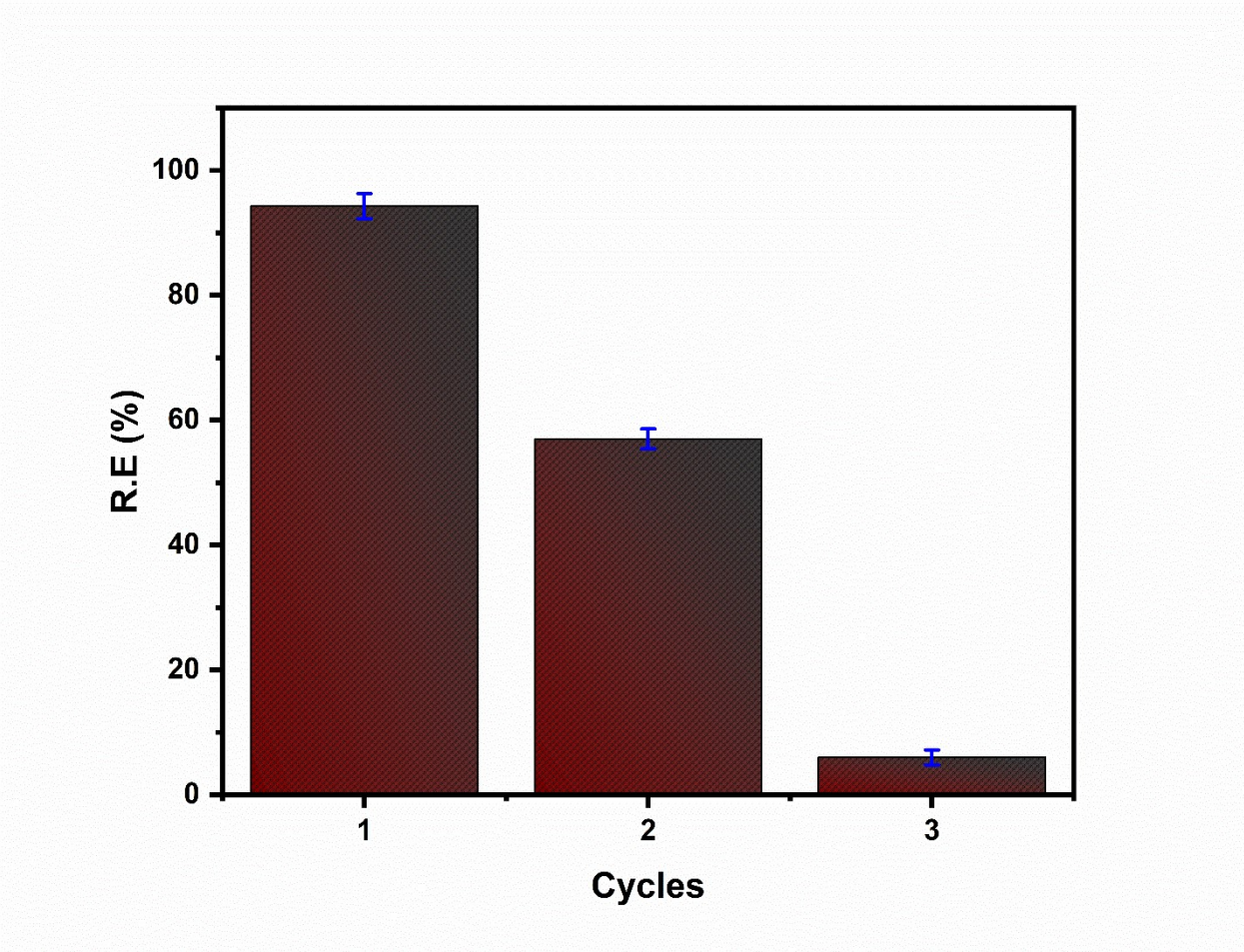

Fig. S22. Reusability of MT-OX COF.

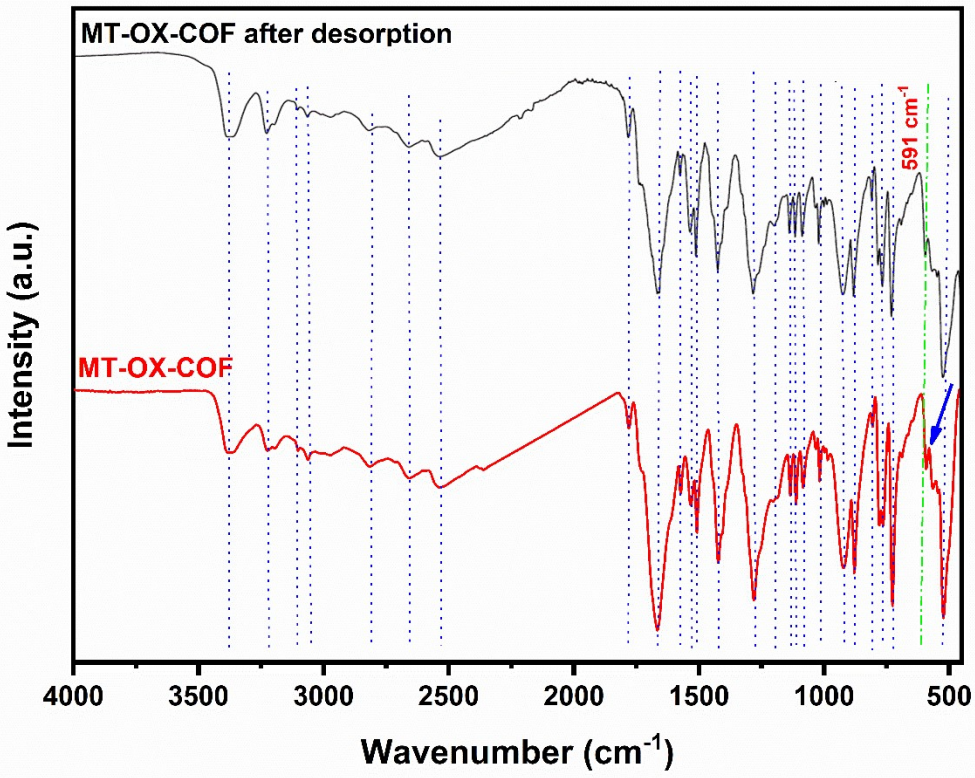

Fig. S23. FT-IR spectra of MT-OX-COF before and after desorption.

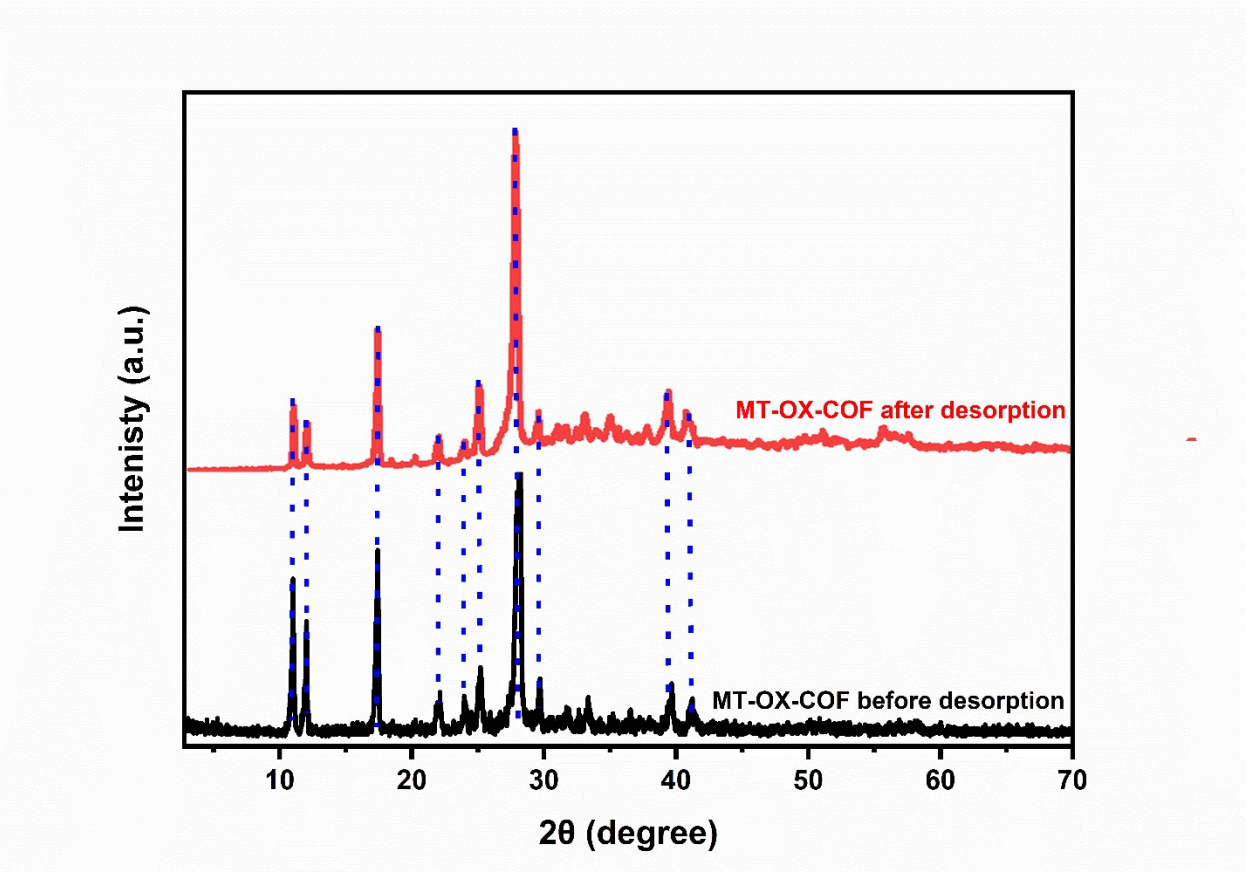

Fig. S24. XRD patterns of MT-OX-COF before and after desorption.

Table S1. Kinetic parameters for sorption of $^{152+154}$Eu onto MT-OX-COF.

Kinetics model	Parameters	Values
Pseudo-first-order	$k_1 \times 10^{-2}$, min^{-1}	2.64
	$q_{e,\ calc.}$, mg g^{-1}	13.24
	$q_{e,\ exp.}$, mg g^{-1}	13.26
	R^2	0.9198
Pseudo-second-order	$k_2 \times 10^{-2}$, g mg^{-1} min^{-1}	0.28
	$q_{e,\ calc.}$, mg g^{-1}	14.46
	$q_{e,\ exp.}$, mg g^{-1}	13.23
	R^2	0.9986
Intra-particle diffusion	k_{dif}, mg g^{-1} $min^{-1/2}$	0.042
	C, mg g^{-1}	12.82
	R^2	0.9475

Table S2. Parameters of the Freundlich, Langmuir, Temkin, and Dubinin–Radushkevich for sorption of $^{152+154}$Eu onto MT-OX-COF.

Isotherm model	Parameters	Values
Freundlich	K_f	13.97
	n	3.90
	R^2	0.9986
Langmuir	Q_m (mg g^{-1})	45.78
	b $\times 10^{-2}$ (L mg^{-1})	45.90
	R_L	0.09
	R^2	0.9674
Temkin	A (L g^{-1})	8.85
	b_t (kJ mol^{-1})	0.381
	B	6.49
	R^2	0.9831
Dubinin–Radushkevich	q_{max} (mg g^{-1})	40.86
	β (mol^2 $kJ^{-2}x10^{-7}$)	3.08
	E (kJ $mol^{-1}x10^{-4}$)	7.85
	R^2	0.9370

Table S3. Thermodynamic parameters for sorption of $^{152+154}$Eu onto MT-OX-COF.

Temperature (K)	ΔG^o (kJ mol^{-1})	ΔH^o (kJ mol^{-1})	ΔS^o (J mol^{-1} K^{-1})
298	0.26		
303	0.31		
313	1.00	-10.45	-0.04
323	1.01		
333	1.90		

2.2. Instruments

Diverse methodologies were used to examine the MT-COF and MT-OX-COF. The characteristics of the produced COFs were analyzed using FT-IR spectroscopy (JASCO 3600 spectrometer) with potassium bromide disks in the ambient temperature range of 400 to 4000 cm^{-1}. The COFs' structure was evaluated by ^{1}H NMR and ^{13}C NMR spectra utilizing a 300 MHz Gemini NMR spectrometer (ECA 500 II, JEOL, Japan). X-ray photoelectron spectroscopy (XPS) yielded elemental composition data via a Thermo Scientific KAlpha XPS spectrometer. The mass spectrum was obtained using a Thermo Scientific quadrupole ISQ meter. Thermal stability was assessed using thermogravimetric analysis (TGA) using an SDT Q600 analyzer in a nitrogen environment. A Bruker AXS D8 diffractometer (Germany) with an improved D_8 X-ray step size and a 0.4 s scan speed in the 2θ range of 3 to 70° was used for XRD analysis, while a JEOL JSM-6510LV scanning electron microscope (Japan) was employed to examine the morphology. BET surface area and pore size distribution were measured using a Quantachrome at 77.35 K. Samples were degassed at 200°C for 6 h. The data was analyzed using Quantachrome TouchWin version 1.2 software. High-resolution transmission electron microscopy (HR-TEM) images were captured using a JEM-2100 camera (JEOL, Japan). The photoluminescence (PL) spectra of the samples were provided using a spectrofluorophotometer (Shimadzu RF-5301PC) at 25^{o}C with an excitation wavelength of 320 nm. The scattering of light through suspension solutions of COF particles in acetone was investigated using a laser beam source (IEC/EN 60825-1 ED-2:2007). A Model 2010 scalar amplifier and a Nucleus Model 500 NaI-Tl scintillator counter were used to provide enhanced resolution in γ channel radiometric studies.

2.3.1. Sorption investigations

Each study was performed until equilibrium was achieved, using a batch technique with three replicates of each experiment. MT-COFs were equilibrated with a $^{152+154}$Eu aqueous solution at several pH values (1-4.25). Multiple variables were examined, including contact duration (5 minutes to 48 hours), the ideal mass ratio of MT-COF, the temperature (25 to 60°C), and the NaCl ionic strength (0.01 to 0.2 mol L^{-1}). A thermostatic shaker facilitated the comprehensive mixing. Centrifugation was used to isolate the liquid phase from the COF, and the radiometric assessment of $^{152+154}$Eu activity was performed. The R.E% of $^{152+154}$Eu was determined using Eq. 1:

$$R.E\% = \frac{A_i - A_f}{A_i} \times 100 \qquad \text{Eq. 1}$$

The activity of the europium active solution was initial denoted by A_i while that after sorption process and was given as A_f. Eq. 2 was used to find the amount of $^{152+154}$Eu that has been bound onto COF (in mg g^{-1}).

$$q_e = \frac{(C_o - C_e) \times V}{m} \qquad \text{Eq. 2}$$

Signs C_o and C_e (mg L^{-1}) show the initial and final concentrations of $^{152+154}$Eu. The amount of COF in grams is (m), and the volume of the solution in liters is (V).

2.3.2. MT-COF regeneration

The radioisotopes desorption process was investigated using different eluents, where 20 mg L^{-1} of $^{152+154}$Eu aqueous solution was mixed with a certain quantity of COF material for six hours at the appropriate pH value. The radiometric activity of the separated supernatants was measured. The solid residues were subsequently mixed with 5.0 mL of each of the 10 eluents: 0.1 mol L^{-1} calcium chloride, strontium chloride, ferric chloride, aluminum nitrate, hydrochloric acid, nitric acid, citric acid, ethylenediaminetetraacetic acid, sodium hydroxide, and distilled water, and then agitated for two hours. Determinations were then performed on the isolated supernatants to measure $^{152+154}$Eu activity. Eq. 3 was used to calculate the percentage of desorption (D%)**:**

$$D\% = \frac{A_d}{A_i - A_F} \times 100 \qquad \text{Eq. 3}$$

In the given equation, A_i and A_F stand for the $^{152+154}$Eu solution's starting and final activities, before and after sorption, respectively. A_d shows the activity of the residue after the desorption process.

Three adsorption-desorption cycles were performed, achieving capacity retention rates of 94%, 57%, and 6% (Fig. S22). To study the significant performance drop after the third cycle, FTIR analysis was employed to examine the structure of MT-OX-COF after desorption using $FeCl_3$ (Fig. S23). The spectra revealed no significant structural differences between the pristine and desorbed MT-OX-COF, indicating that the adsorption–desorption processes did not alter the framework structure. This confirms that MT-OX-COF retains its structural stability throughout the adsorption–desorption cycles. A minor shift was observed at 591 cm^{-1} in the desorbed MT-OX-COF compared to the pristine one, which may be attributed to ionic exchange between Eu^{3+} and Fe^{3+} ions during desorption. This interaction was further supported by the color change of the MT-OX-COF from colorless to faint brown after desorption. In addition, the XRD analysis reveals that there was no significant change in the structure of the MT-OX-COF before the Eu(III) sorption, and after the desorption step using $FeCl_3$ (Fig.S24). This is strong evidence of the stability of the MT-OX-COF, and there is no structure degradation. Also, a gravimetric quantitative analysis was conducted to compare the mass of the COF before and after desorption. The results showed no significant difference in the initial and final masses, which were both 0.03 g, confirming that the MT-OX-COF maintained its structural integrity without degradation during the adsorption–desorption process. Thus, the decline in performance is likely due to framework saturation with Fe^{3+} ions during repeated desorption, not related to the structure degradation.

2.3.3. Radioactivity determination and real waste preparations

2.3.3.1. Radioisotope preparation

$^{152+154}$Eu was obtained by neutron activation through neutron irradiation of an accurate weight of Eu_2O_3. The target europium powder was wrapped using a high-purity aluminum foil, which was placed in a can and allowed for neutron irradiation with a flux of 1×10^{14} n cm^{-2} sec^{-1} for 48 h through the 22 MW Egyptian research reactor ARE-RR-2 in Inshas (Cairo). After activation of europium, it was left for a time to cool, then it was dissolved in a certain amount of hydrochloric acid (1 mol L^{-1}). The solution was evaporated to obtain europium chloride salt, which was then dissolved in double-distilled water and used as a tracer in the present work.

2.3.3.2. Real study samples

The removal behavior of the MT-OX-COF was investigated toward a real waste from the atomic energy authority, which had an initial pH of 3.5. The waste sample contained cesium, europium, iodine, molybdenum, strontium, and technetium isotopes.